Delft University of Technology

Viscoelastic effects on residual oil distribution in flows through pillared microchannels

De, S.; Krishnan, P.; van der Schaaf, J.; Kuipers, J. A.M.; Peters, E. A.J.F.; Padding, J. T.

Important note
To cite this publication, please use the final published version (if applicable).
Please check the document version above.

Viscoelastic effects on residual oil distribution in flows through pillared microchannels

S. De[1], P.Krishnan[1], J. van der Schaaf[2], J.A.M. Kuipers[1], E.A.J.F. Peters[1], J.T. Padding[3],*

1 Multiphase Reactors Group, Department of Chemical Engineering and Chemistry,
Eindhoven University of Technology, The Netherlands
2 Chemical Reactor Engineering Group, Department of Chemical Engineering and Chemistry,
Eindhoven University of Technology, The Netherlands
3 Process & Energy department, Delft University of Technology, The Netherlands
* Corresponding author, Tel +31 15 2786605, e-mail: J.T.Padding@tudelft.nl

Abstract

Hypothesis

Multiphase flow through porous media is important in a number of industrial, natural and biological processes. One application is enhanced oil recovery (EOR), where a resident oil phase is displaced by a Newtonian or polymeric fluid. In EOR, the two-phase immiscible displacement through heterogonous porous media is usually governed by competing viscous and capillary forces, expressed through a Capillary number Ca, and viscosity ratio of the displacing and displaced fluid. However, when viscoelastic displacement fluids are used, elastic forces in the displacement fluid also become significant. It is hypothesized that elastic instabilities are responsible for enhanced oil recovery through an elastic microsweep mechanism.

Experiments

In this work, we use a simplified geometry in the form of a pillared microchannel. We analyze the trapped residual oil size distribution after displacement by a Newtonian fluid, a nearly inelastic shear thinning fluid, and viscoelastic polymers and surfactant solutions.

Findings

We find that viscoelastic polymers and surfactant solutions can displace more oil compared to Newtonian fluids and nearly inelastic shear thinning polymers at similar Ca numbers. Beyond a critical Ca number, the size of residual oil blobs decreases significantly for viscoelastic fluids. This critical Ca number directly corresponds to flow rates where elastic instabilities occur in single phase flow, suggesting a close link between enhancement of oil recovery and appearance of elastic instabilities.

Keywords: Enhanced Oil Recovery; displacement fluid; viscoelastic instability; oil droplet size distribution

1 Introduction

Multiphase fluid flow through porous media is of high importance in a large number of industrial and physical processes, such as enhanced oil recovery, soil remediation, geophysical, biological and engineering applications [1,2]. The flow of a single-phase Newtonian fluid through a porous medium is well understood within the framework of Darcy's law in the creeping flow regime. However, multiphase flow through porous media involving non-Newtonian fluids are much more complex in nature [1]. In enhanced oil recovery, both water

and polymer solutions are pushed through the porous media, to displace oil from reservoirs. Because the pore length scales and fluid velocities are small, the Reynolds number is usually small. However, two other non-dimensional numbers become very critical in such immiscible transport processes. The first one is viscosity ratio (M), defined as the ratio between the viscosities of displacing and displaced fluid. A value of M > 1 is considered favorable, while M < 1 is unfavorable for displacement because of appearance of viscous fingering instabilities. The second important number is the capillary number Ca, defined as the ratio of viscous and surface tension forces $Ca = \mu u / \sigma$. Here μ is the viscosity of the displacing fluid, u is the Darcy velocity, and σ represents the interfacial tension between the displacing and displaced fluid. Substantial experimental and numerical work has been done by researchers to understand the influence of Ca, M, and wettability on displacement efficiency [3–13].

In case of water flooding, the viscosity ratio, M is generally <1. Thus, after water flooding a large amount of oil remains non-displaced. Large disconnected islands of oil, called ganglia, remain trapped in the porous medium. In such cases, due to the heterogeneity of the rock structure and difference in permeability, preferential flow paths for the water are formed, which causes less recovery. As a next stage of oil recovery, non-Newtonian fluids are injected into the oil reservoir. One of the features of such fluids is that the viscosity depends on the local shear rate. Thus the Ca number is redefined as $Ca = \mu(\gamma)u / \sigma$, where $\dot{\gamma}$ is a typical (or dominant) shear rate in the porous medium. The viscosity ratio $M = \mu(\gamma)/\mu_d$ also changes, depending on the local shear rate. Here μ_d is the viscosity of the displaced fluid. Non-Newtonian fluids that are commonly used in enhanced oil recovery include hydrolyzed polyacrylamides (HPAM), xanthan gums, and viscoelastic surfactants (VES) [2,14]. The typical Ca numbers in oil field applications range from 10^{-5} to 10^{-3} [2,5]. Generally, with increasing Ca the displacement efficiency increases. However, a non-monotonic dependence of Ca number on residual oil saturation was recently reported [3,15]. Non-Newtonian fluids are found to recover more oil than their Newtonian counterparts [16] *for a similar range of Ca numbers*.

Previous research suggested that flooding by non-Newtonian fluids can only improve the macroscopic sweeping [17], i.e. displacement of oil on scales much larger than that of individual pores. However, current research work [18–22] and field studies [16] suggest that non-Newtonian fluids might increase oil recovery by microscopic oil displacement on the scale of a single or a few pores, sometimes referred to as micro-sweep. Of course, even for a Newtonian displacement fluid such as water, mobilization of the ganglia may occur beyond a critical Ca number [23]. However, for non-Newtonian displacement fluids, viscoelastic effects can mobilize the oil ganglia at *lower* Ca numbers. Viscoelastic effects already occur during *single* phase flow of non-Newtonian fluids through porous media. The important non-dimensional number characterizing the importance of elastic effects is the Deborah number De, defined as the ratio of the fluid relaxation time and a characteristic time scale of the flow experiment. Non-Newtonian fluid sometimes exhibit time dependent velocity fluctuations in the flow fields which are reminiscent of turbulence, however they occur at very small Reynolds number, a phenomenon called elastic turbulence [24–26]. Elastic instabilities occur when the De number is sufficiently large, as reported experimentally for both polymeric [24,27–32] and

wormlike micellar solutions [33–39]. Numerical simulations also show the presence of such spatial and temporal elastic instabilities [26,40–42]. Our recent simulations of viscoelastic flow through symmetric and asymmetric set of cylinders and through a random porous medium show that the origin of these instabilities are more related to the viscoelastic shear stress than to extensional contributions [25,43]. Recent findings by Clarke et al. [18] , Avendano et al. [44] and Nilsson et al. [45] show the possible effects of viscoelasticity in enhanced displacement. Rodriguez de Castro et al. [46] very recently showed effects of shear thinning fluids on residual oil formation. However, a complete picture regarding the residual oil size distribution and its correlation with viscoelasticity is still missing.

In this work, we will show that the enhanced oil recovery by micro-sweep observed in *two-phase* flows through porous media is strongly correlated with the appearance of elastic instabilities observed in *single phase* flows of the same displacement fluid through the same porous medium. Our work therefore suggests that *elastic* instabilities, rather than e.g. shear-thinning or other quasi-Newtonian effects on the viscosity, are responsible for the enhanced micro-sweep for the set of fluids investigated in this study.

Displacement experiments are often performed on fully three-dimensional rock core samples. However, detailed visualization of the phases on the level of the rock pores is extremely difficult. Instead, we use a microchannel with a strategic arrangement of cylindrical pillars, ensuring that the time and length scales are similar to those occurring in actual rock structures [47]. Several researchers have shown that multiphase flow studies are possible (and relevant) in such microchannels [3,48,49]. In this study, we compare a Newtonian fluid (water) with three types of non-Newtonian fluids, namely a slightly elastic shear thinning fluid (xanthan), a viscoelastic shear thinning polymer (hydrolyzed polyacrylamide - HPAM), and a viscoelastic surfactant (VES), for their ability to displace oil in the microchannel in a similar range of Ca numbers. The reader should note that in the definition of Ca number the viscosity $\mu(\gamma)$ is obtained from the single phase microfluidic experiments. A detailed analysis of the ganglia size distribution shows that both HPAM and VES are able to fragment large oil ganglia to smaller microstructures. The Ca number where the micro-sweep increases significantly corresponds to flow rates where increased flow resistance and elastic instabilities are observed in single phase viscoelastic fluids. Water and xanthan showed no such micro-sweep displacement patterns for similar Ca ranges.

This paper is organized as follows. In section 2 we detail the microfluidic setup, give details of the bulk rheology of the fluids used in this study, and explain the experimental procedure. In section 3 we show and discuss our results. In section 4 we end with our conclusions.

2 Material and methods

2.1 Microfluidic setup

The displacement experiments are performed using a pillared microchannel. A porous medium is mimicked by strategically placing an array of cylindrical pillars in a hexagonal pattern from the entry to the exit of the microchannel, as shown in figure 1. These pillars act as obstacles in the flow path, creating continuous contraction and extension of the displacing fluid. The straight

microchannels are 6.6 cm long, with a width and height of 1 mm and 50 µm, respectively. The distance along the flow direction (x) between the surfaces of two successive pillars (X_p) and along the width (y) of the channel (Y_p) are 4 µm and 1 µm, respectively. The pillar diameter (D_p) is 3 µm. This results in a porosity (ϵ) of 0.75. The number of pillars along x and y direction is 10000 and 240 respectively. The channel and cylinders are etched in silicon. All pillars are modified with a hydrophilic coating and microchannels are fabricated using a photolithography technique. A detailed description of the manufacturing of the microchannel is reported in the work of Loos et al [50]. The permeability (k) of the microchannel is determined by flowing water through the pillared microchannel and measuring the resultant pressure drop, resulting in $k = 1.0 \times 10^{-11}$ m^2 with an accuracy of ± 2 %. The flow rate is slowly altered and the subsequent pressure drop is measured for the flow of different non-Newtonian fluids in the pillared microchannel. Taking the square root of permeability as the length scale, an apparent shear rate and apparent viscosity can be calculated from these measurements (explained later). These can be further used, to calculate the Capillary number knowing the interfacial tension of the different fluids under consideration.
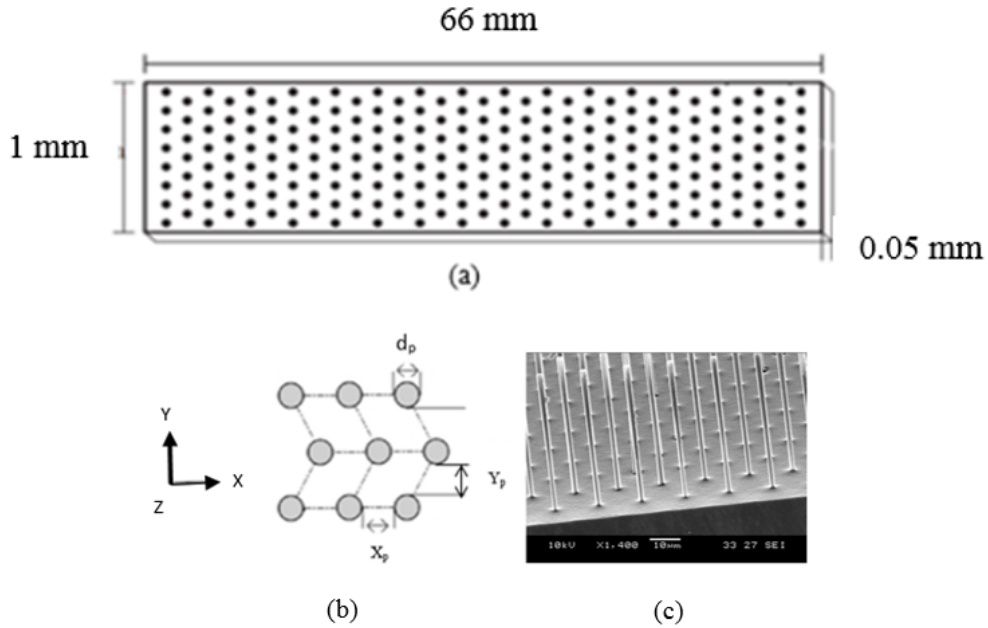

Figure 1. Geometry of the pillared microchannel: (a) channel geometry with dots showing the pillar locations. Flow is from left to right (x-direction). Planar walls are present at both sides in the width (y) and height (z) direction; (b) arrangement of pillars, indicating the distances between pillars X_p and Y_p; (c) SEM image of a typical pillared channel (arrangement and structure of a typical pillar is shown)

2.2 Fluid characteristics

A Newtonian silicone oil of dynamic viscosity 0.02 Pa s (Sigma Aldrich) is used as the displaced fluid in all of our experiments. As a displacing fluid, Newtonian and non-Newtonian fluids are used over similar ranges of Ca number. The displacing fluids are all immiscible with the displaced oil.

First, water is used as the Newtonian displacing fluid. The water has a viscosity of 0.001 Pa s. The oil-water interfacial tension, measured using a digital Kruss surface tensiometer is around 30 ± 1 mN/m.

Second, as a pseudoplastic shear thinning displacing fluid, xanthan is used. Xanthan is extensively used in the industry as a food additive and a viscosifying agent [51]. A xanthan solution of concentration 225 ppm is prepared by addition of xanthan in distilled water with careful stirring to obtain uniform mixing. The viscosity of the xanthan solution was measured with an Anton Paar MCR 302 series rheometer. The zero-shear viscosity (η_0) of the xanthan solution is 0.06 Pa s, as characterized by the standard strain controlled double gap rheometer at room temperature (22^0C). The xanthan solution has a shear thinning rheology as shown in the rheogram of figure 2. At lower shear rates a Newtonian-like plateau region is observed, followed by a shear thinning part. The viscosity profile obtained here is similar to other literature results [52]. The oil-xanthan interfacial tension was found to be around 28 ± 1 mN/m similar to that of the oil-water system.

Third, as a viscoelastic shear thinning displacing fluid, hydrolyzed polyacrylamide solution (HPAM) is used. HPAM is often used in polymer flooding operations and is considered to have high elastic effects for the molecular weight (20 MDa) used this study [16]. The solution is prepared by adding 2000 ppm of HPAM 3630S and 1 weight-% of salt (NaCl) in deionized water solution. At these concentrations, the zero-shear viscosity (η_0) of the HPAM solution is approximately 0.05 Pa s, similar to that of the xanthan solution. The rheology of the HPAM solution is also measured using the strain controlled rheometer. The steady shear rheology of the HPAM solution is shown in figure 3. A rheological characterization of similar HPAM solutions has been performed in detail in the recent work of Howe et al. [19]. The oil-HPAM interfacial tension was determined to be 29 ± 1 mN/m.

We have fitted the steady shear rheology data of both xanthan and HPAM with the Carreau-Yasuda (CY) model [53]. The CY model describes the Newtonian plateau and shear thinning behavior of HPAM accurately,

$$\eta\left(\dot{\gamma}\right) - \eta_\infty = \left(\eta_0 - \eta_\infty\right)\left[1 + \left(\lambda\dot{\gamma}\right)^a\right]^{\frac{(n-1)}{a}} \tag{1}$$

where η is the shear rate dependent viscosity, η_∞ is the infinite shear viscosity, λ is the relaxation time, n is the power law index, and a is a parameter describing the rate of transition from the Newtonian plateau to the power law region. Table 1 shows the fit parameters from the CY model with the accuracy of the fit. At very low and high shear rates the shear rheology measurements becomes inaccurate especially with low viscosity solutions. Thus the rheological parameters are determined with the CY model. The rheological experiments have been repeated over time, to observe any possible polymer degradation. In our experimental time frame no polymer degradation was found.
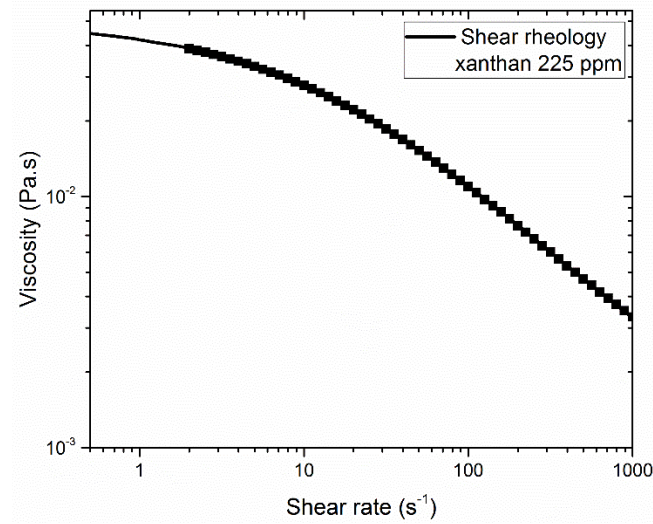
Figure 2. Steady shear viscosity vs. shear rate for the xanthan solution, fitted with the CY model
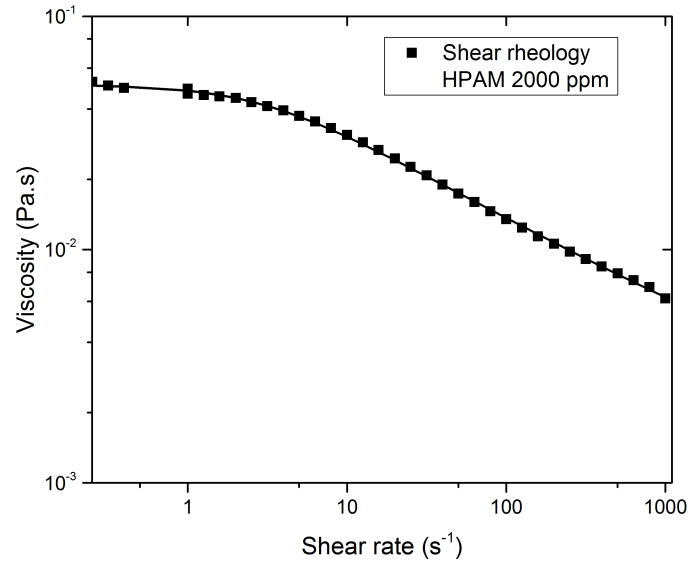

Figure 3. Steady shear viscosity vs. shear rate for the HPAM solution, fitted with the CY model

Table 1. Rheological parameters from Carreau – Yasuda model

Fluids	λ (s)	n	a	η_0 (Pa.s)	η_∞ (Pa.s)
Xanthan	5.0×10^{-2} $\pm\,1.0\times10^{-3}$	2.5×10^{-1} $\pm\,5.0\times10^{-3}$	6.2×10^{-1} $\pm\,4.0\times10^{-3}$	4.9×10^{-2} $\pm\,2.0\times10^{-4}$	1.0×10^{-3}
HPAM 3630	3.0×10^{-1} $\pm\,2\times10^{-2}$	5.8×10^{-1} $\pm\,1\times10^{-2}$	1.07 $\pm\,7\times10^{-2}$	5.0×10^{-2} $\pm\,4.0\times10^{-4}$	1.0×10^{-3}

Finally, a viscoelastic surfactant (VES) solution is used as the displacing fluid. Surfactants are amphiphilic molecules, consisting of a hydrophilic head and a hydrophobic tail group. When the surfactant concentration is higher than the critical micelle concentration (CMC), the surfactants spontaneously self-assemble to form micelles. For certain types of surfactants, these self-assembled structures are in the form of wormlike micelles. Wormlike micelles are often referred to as 'living polymers' [54] because, like polymers, at higher concentrations they can form entangled networks leading to a viscoelastic fluid. In contrast to polymers however, wormlike micelles do not have a covalently bonded backbone [55]. Instead, they are held together by relatively weak physical forces which continuously break and reform [56]. The rheological characteristics of VES are believed to be beneficial for enhanced oil recovery and are currently explored in the oil industry.

In this work, a VES solution is prepared by adding 2.0 mM of cationic surfactant cetyltrimethylammonium bromide (CTAB) and 2.0 mM of the organic salt sodium salicylate (NaSal) to de-mineralized water with 3% NaCl. The rheology of this VES is analyzed using a similar procedure as for xanthan and HPAM with a stress controlled rheometer. As shown in figure 4, at low shear rates (<100 s^{-1}) the VES shows a more-or-less Newtonian plateau. After a critical shear rate of 450 s^{-1}, a shear thickening behavior is observed, followed by shear thinning at very high shear rates (>1000 s^{-1}). This peculiar rheological response is the consequence of a competition between continuous formation and destruction of the macromolecular network structure in the VES solution. Because both formation and destruction are strongly influenced by shear flow, these network structures are also referred to as shear induced structures (SIS) [34]. The oil-VES interfacial tension was determined to be 20 $\pm$ 0.5 mN/m.
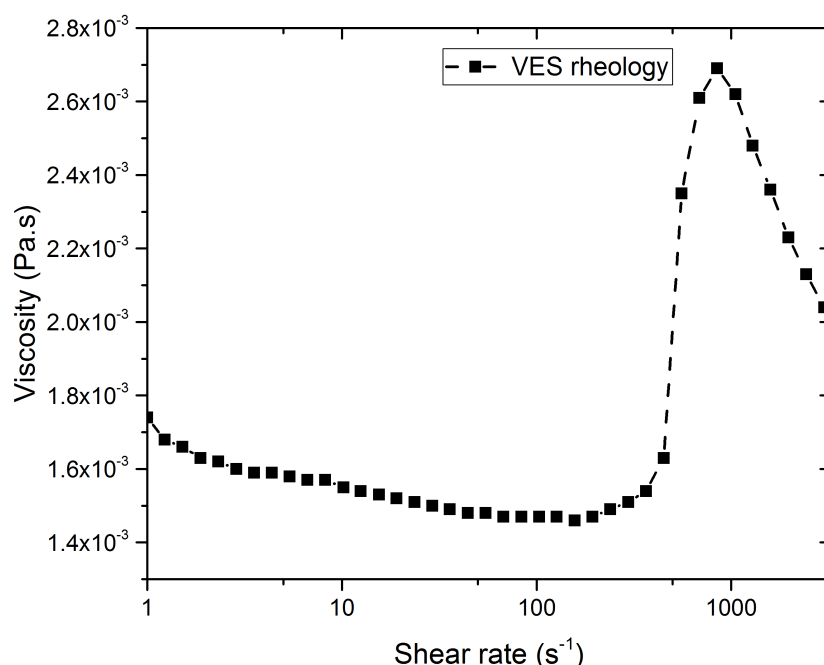

Figure 4. Steady shear viscosity vs. shear rate for the VES solution

2.3 Experimental method

The displacement experiments are conducted for Ca numbers typically ranging from 5×10^{-6} to 10^{-3}. At the start of experiment, the silicone oil is mixed with Sudan red dye (Sigma Aldrich). The solution is passed through a small bed with filters to remove any agglomerates which might block the microchannel. Then a clean pillared microchannel is saturated completely with the dyed silicone oil, using a KR analytical syringe pump (Fusion 200 Touch, KR analytical Ltd, UK). The injection flow rate of the pump ranges from $10^{-13} - 10^{-8}$ m^3/s. Care is taken to avoid any air bubbles in the microchannel at this stage. Then the oil is displaced by injecting the displacing fluid, over a range of different flow rates. A Sensor Technics micro pressure sensor (Puchheim, Germany) is connected to the channel to measure the pressure drop over the channel. The range is 0 to 2 bar, with a temporal resolution of 1 ms. The experiments are stopped when a steady state is reached. A steady state is defined here as a state in which a steady pressure is shown by the pressure sensor and no further displaced oil is found at the outlet. Each experiment is repeated three times, to check the reproducibility of the results and estimate error bars. Because multiple fluids are used during the course of the experiments, a detailed cleaning procedure is followed before the start of any experiment. The microchannel is first rinsed with deionized water, followed by isopropanol and deionized water. After this cleaning step, each channel is dried by injecting pressurized air.

The pillared microchannel is placed on a Zeiss Axio Observer D1 inverted microscope. After the experiment has reached steady state, the flow is stopped and a series of images is captured from the channel entry to channel exit using a Redlake Motion Pro X-4 camera mounted on the top of the microscope. Individual images are obtained in a square section (around 66% of the channel width), centered around the middle of the channel. The experimental set up is similar to the set up described in the work of Sousa et al. [57]. A set of images is also taken before the injection of the displacing fluid, as a reference. To investigate the microstructure of the residual oil ganglia, a detailed analysis of the obtained images is performed, as described in detail by Meyer et al. [58]. The reference image is first subtracted from the steady state images. The residual images are then analyzed with the region of interest tool in Matlab. With this tool, the region in the microchannel which is filled with oil ganglia is identified. These regions are then converted to corresponding binary images. The residual oil saturation (S_{ro}) is then calculated as the percentage of microchannel filled with the oil phase. The images are further analyzed to investigate the distribution of shape and size of the residual oil ganglia.

Apart from the two-phase displacement experiments, a set of single phase experiments for each displacing fluid through the same pillared microchannel is also performed over a wide range of flow rates. The pressure drop data from these experiments are used to obtain the viscosity vs. apparent shear rate, using Darcy's law.

3 Results and discussion

3.1 Displacement results

Figure 5 shows a comparison between the percentage oil saturation (i.e. the percentage oil remaining in the microchannel at steady state) as a function of Ca number for different

displacing fluid namely water, xanthan, HPAM and VES. The figure shows that the viscoelastic HPAM solution can recover more oil at most Ca numbers than the Newtonian water and slightly elastic shear thinning xanthan solution. The VES solution also shows a good recovery, almost comparable to that of HPAM. The critical Ca, defined as Ca number where the oil saturation is 25% (where the oil saturation decreases most rapidly with increasing log(Ca) in Fig. 5), is around 4×10^{-5} for HPAM flooding and around 7×10^{-5} for VES flooding. However, for xanthan and water based flooding the critical Ca is around 2×10^{-4} and 3×10^{-4}, respectively. The mobility ratio (M) for the water-oil system is much less than 1, which may explain the lower recovery. The mobility ratio for the xanthan-oil and HPAM-oil systems (based on the zero-shear viscosity) are both around 3. The enhanced displacement of HPAM, relative to xanthan, must thus be related to the much stronger viscoelastic effects of the HPAM solution. In the case of the VES, the value of M is less than 1, while the displacement is nevertheless in between that of xanthan and HPAM. This relatively high displacement capability of VES further strengthens our conclusion that viscoelastic effects must be responsible for the enhanced oil recovery.
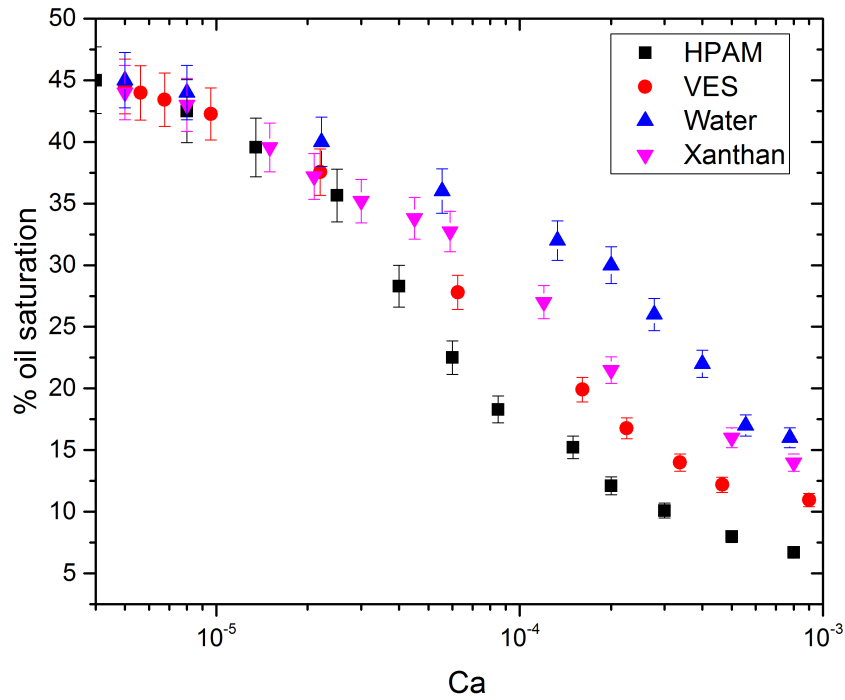

Figure 5. Percentage remaining oil saturation as a function of capillary number for different displacing fluids. Error bars show the variability between 3 experiments.

3.2 Ganglia size distribution

To understand the detailed mechanism behind the observed enhanced oil displacement more clearly, snapshots of the residual oil microstructures are given in figure 6. The representative snapshots are selected such that all figures are in a comparable range of Ca numbers for the different displacing fluids. At lower Ca numbers (10^{-5}), large blobs of residual oil remain in place, irrespective of the type of displacing fluid. For intermediate Ca numbers (10^{-4}), large oil ganglia remain when water or xanthan are used to displace the oil. However, for both HPAM and VES the residual oil ganglia are found to be much smaller in size. At even higher Ca numbers (10^{-3}), the residual oil ganglia are further reduced in size for both HPAM and VES

displacing fluids, while they generally remain large for xanthan and water. In the water-oil system large disconnected oil ganglia are observed, similar to the findings of Datta et al. [23]. The decrease of ganglia size due to viscoelastic effects was also shown qualitatively in the work of Clarke et al. [18,59], analogous to our findings. These experiments conclusively show that at higher Ca (10^{-4} to 10^{-3}), both HPAM and VES can create and mobilize smaller micro oil-droplets.

Figure 7 shows histograms of the oil ganglia size distribution for different Ca numbers and each of the displacing fluids. This figure shows that for all displacing fluids the residual oil size decreases with increasing Ca. However, the histograms also clearly show that for Ca numbers in the range from 10^{-4} to 10^{-3}, the residual oil size distribution is much narrower (with a width of approximately $1 \times 10^4 \, \mu m^2$) for both HPAM and VES, compared to the still rather broad distribution (2 to $5 \times 10^4 \, \mu m^2$) for water or xanthan. Thus, for Ca numbers larger than 10^{-4}, both HPAM and VES can break larger oil ganglia into smaller micro droplets. In a similar Ca range, the shear thinning xanthan solution, while having a similar zero-shear viscosity as HPAM, is incapable of displacing oil with a similar efficiency. The residual oil ganglia are much larger for xanthan displacement, and comparable to the droplet size after water displacement. For water the residual trapped oil droplets are in the form of long narrow strips, whereas for xanthan the residual droplets are disconnected blobs at higher Ca ranges ($>10^{-4}$). At the highest Ca numbers, the droplet size distribution for HPAM is narrower than for VES. This also corresponds to the lowest residual oil saturation by HPAM shown in figure 5.
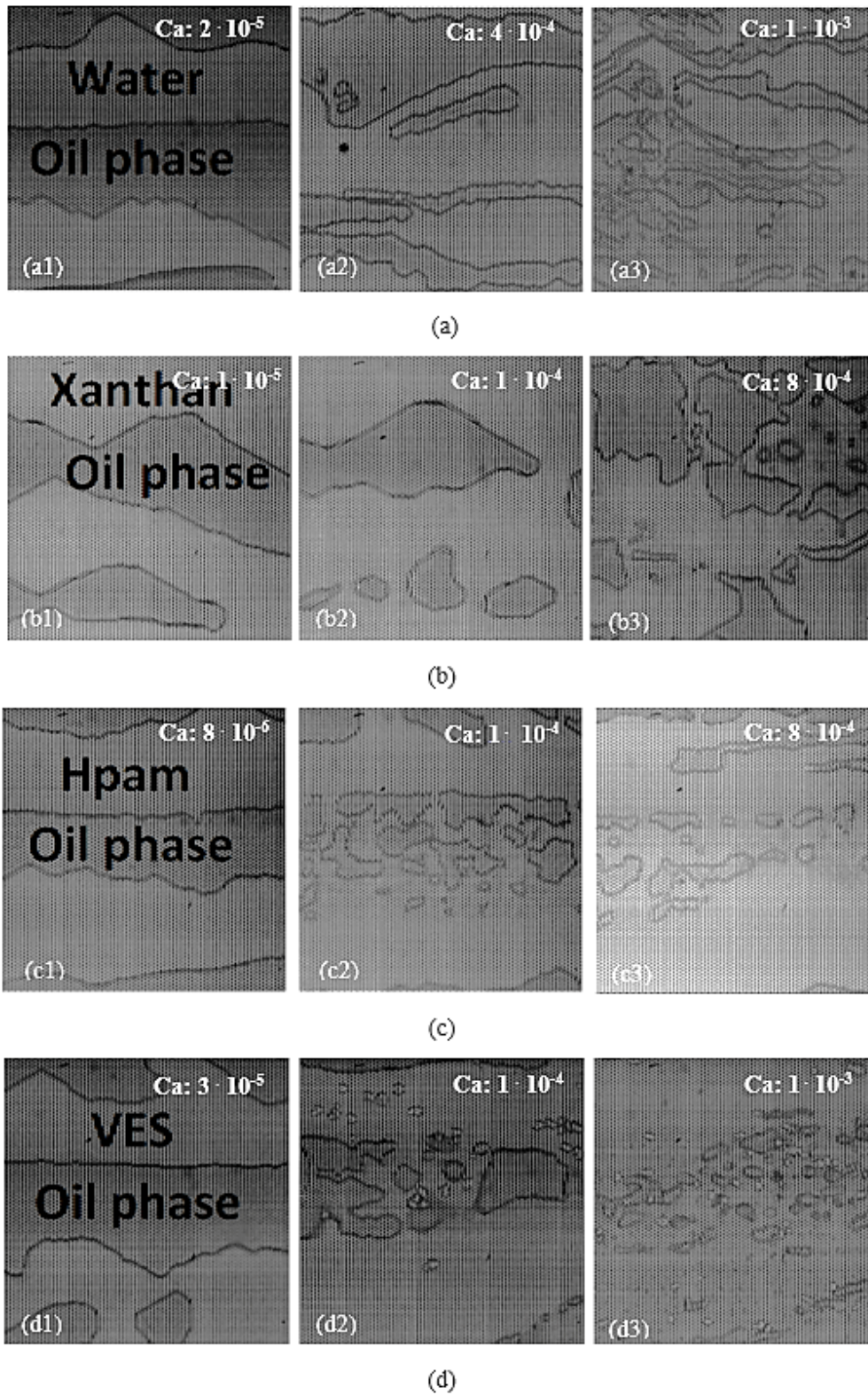
Figure 6. Snapshots of residual oil microstructures in steady state after displacement by (a) water, (b) xanthan, (c) HPAM, and (d) VES. The subfigures (1, 2 and 3) correspond to increasing Ca numbers.
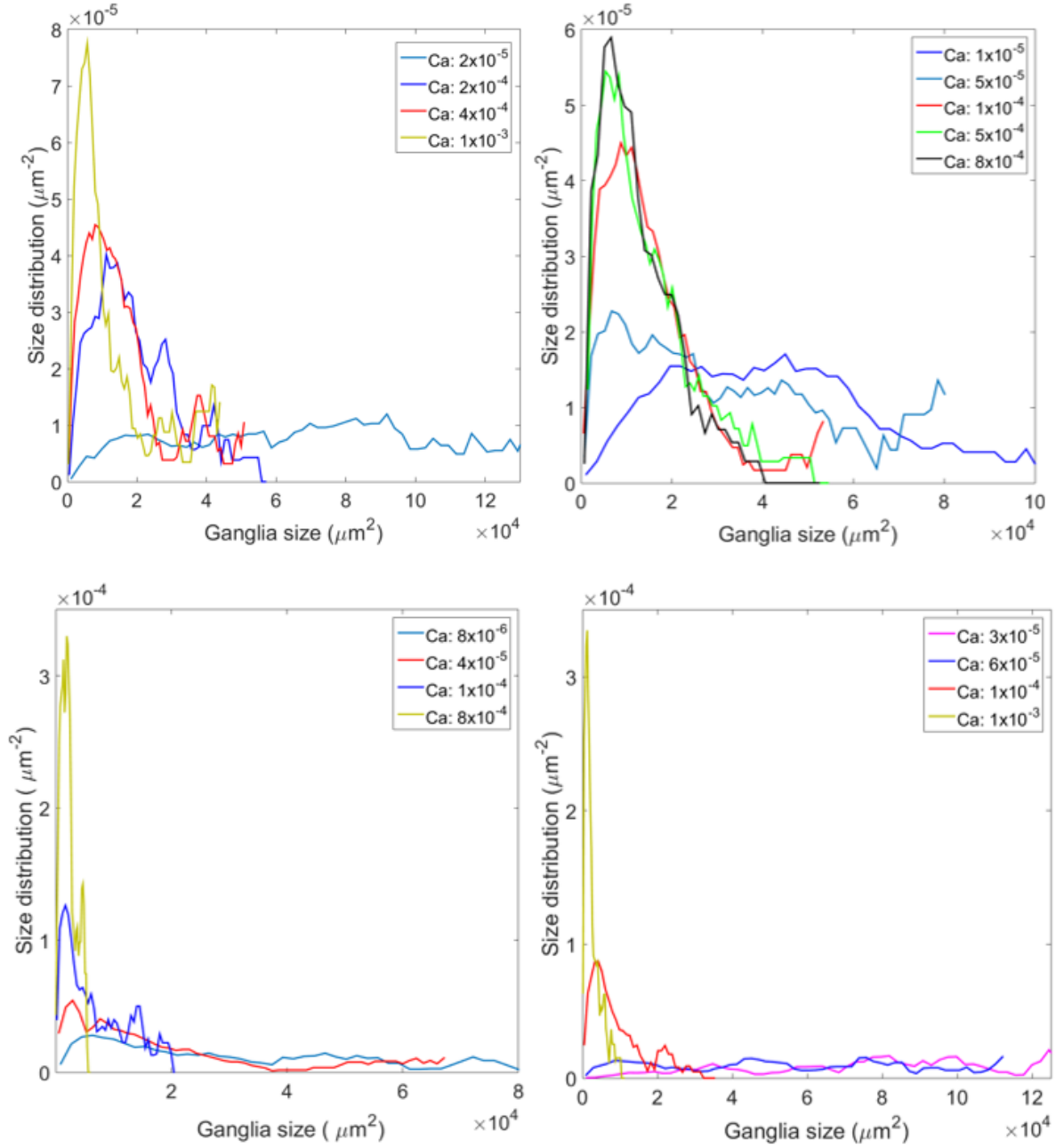
Figure 7. Steady state residual oil size distribution after displacement by (a) water, (b) xanthan, (c) HPAM, and (d) VES. Different colors correspond to difference Ca numbers.

Rodriguez de Castro et al. [46] used a percolation theory concept to correlate the size distribution of trapped non-wetting ganglia after displacement at very low flow rates. They found that the size distribution obeys a power law behavior. The power law exponent from our analysis is around 2 (not shown), similar to the findings of Rodriguez de Castro et al. [46].

3.3 Relation between single and multiphase experiments

In the previous subsection, we have found that oil recovery can be enhanced by micro-sweep, i.e. by microscopic oil displacement on the scale of a few pores, and that this micro-sweep *only* occurs for displacing fluids with an elastic component. The next question is exactly how much

elasticity is necessary. To this end, we now turn to the *single phase* experiments and study the change of viscosity with apparent shear rate, because it is known that the apparent viscosity for flow through a porous medium has a sharp increase when elastic effects start to dominate [25].

For the flow of different non-Newtonian fluids, the steady state pressure drop ΔP over the microchannel of length L was measured for a range of volumetric flow rate *q*. According to Darcy's law, the apparent viscosity, η_{app} can be derived from the pressure drop as follows:

$$\left(\frac{\Delta P}{L}\right) = \frac{\eta_{app}\langle u \rangle}{k} \tag{2}$$

Here *k* is the permeability, which is related to the pore size distribution and tortuosity of the porous medium itself. The permeability *k* is obtained using Darcy's law for the flow of a Newtonian fluid (water) through the pillared microchannel.

The apparent shear rate is defined as $\dot{\gamma} = \beta\langle u \rangle/\sqrt{k}$. Where β is an empirical shift parameter which depends on the pore structure and fluid rheology. In our experiments, we found a good match between the viscosity obtained from the shear rheometer data and single phase experiments through the pillared microchannel using the value of β = 1.0. This is in accordance to the recent findings of Clarke et al. [18] and Rodriguez de Castro et al. [46]. Some researchers found a good correspondence between experimental and numerical observations using a value of β = 2.4 [52]. In our case, for the range of shear rates studied, the polymers do not undergo any mechanical degradation and wall slip is also negligible thus the value of β is found to be 1.0.

The important non-dimensional number characterizing the importance of elastic effects is the Deborah number De, defined as the ratio of the fluid relaxation time and a characteristic time scale of the flow experiment. In this case the characteristic time scale of the flow experiment is the inverse apparent shear rate, leading to $De = \lambda\dot{\gamma} = \lambda\langle u \rangle/\sqrt{k}$.
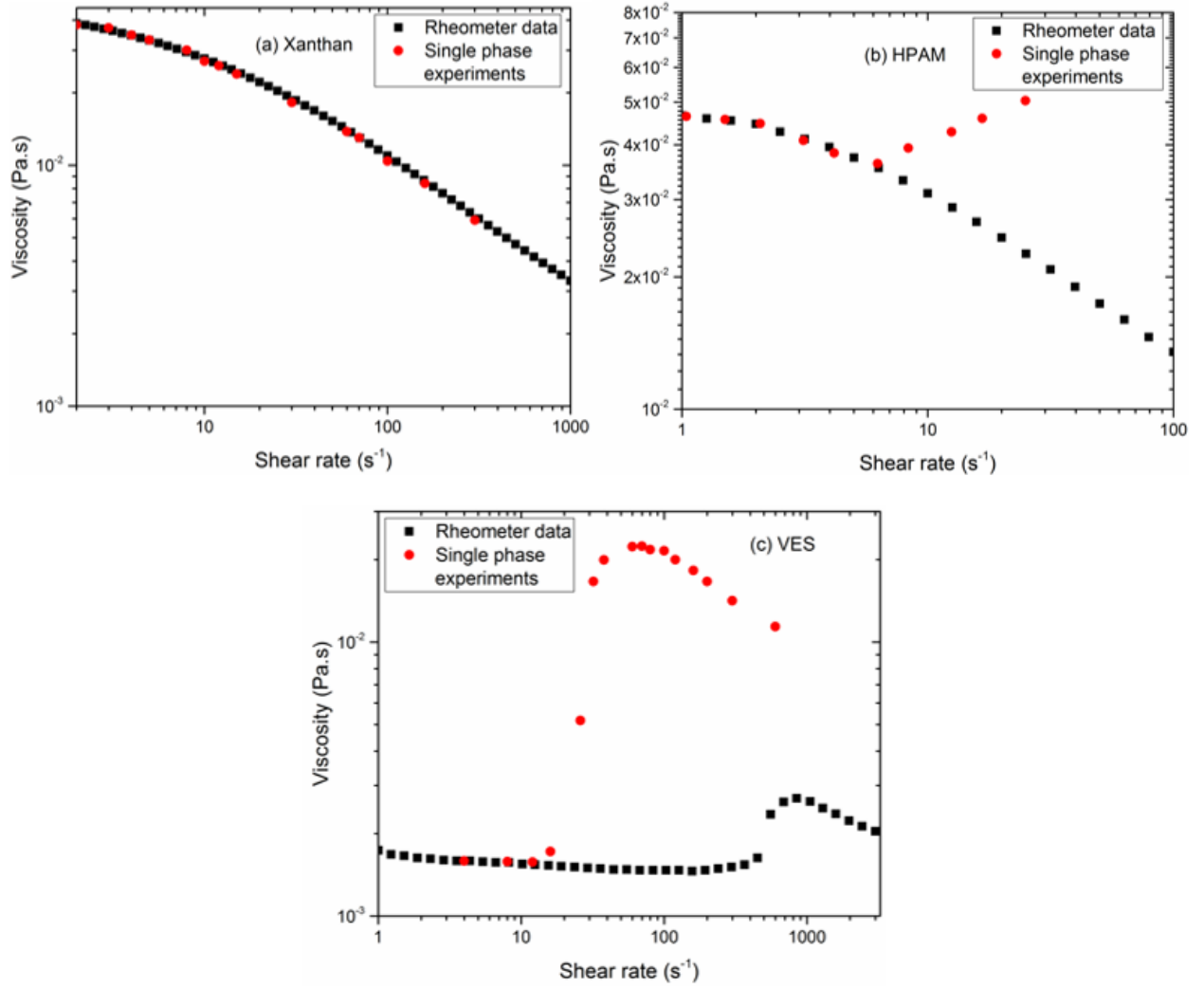
Figure 8. Apparent viscosity from single phase flow through the pillared microchannel (red circles) and from the shear rheometer (black circles) as a function of (apparent) shear rate for different displacing fluids: (a) xanthan, (b) HPAM, (c) VES.

As shown in figure 8, for the xanthan solution, the viscosity as derived from the single phase experiments continuously decreases with increasing shear rate. This corresponds to the shear thinning nature of xanthan, as found from the shear rheology experiments. On the other hand, the viscosity of HPAM initially decreases and then starts to increase after a critical shear rate of around 6 s^{-1}. So, although the bulk shear rheology experiments show that HPAM is shear thinning, it shows an increased apparent viscosity when flowing through a porous medium at higher flow rates. In case of the VES solution, the viscosity derived from single phase experiments shows shear thickening followed by shear thinning behavior, qualitatively similar to what was found in the shear rheometer. However, the critical shear rate where the shear thickening starts (20 s^{-1}) is at a much lower shear rate, compared to the rheometer predictions. Also, the extent of shear thickening (ratio between maximum and minimum viscosity) for VES is approximately 14 times in the pillared microchannel, compared to 2 times in the shear rheometer. The increased flow thickening for the flow of VES solution in the pillared microchannel also matches with the findings of Rojas et al. [36].

Viscoelastic effects induce strong spatial and temporal instabilities and even lane changes, as shown in our work [32] on flow of HPAM solutions through pillared microchannels of similar configurations. The occurrence of such elastic instabilities in model porous media for HPAM was also shown in the work of Clarke et al. [18], Kawale et al [60] and other researchers. Also for the VES solutions, recent studies of Zhao et al. [61], Moss et al. [55], and De et al. [39] show that after a critical shear rate flow instabilities occur when flowing through a model porous medium. This elastic instability and excess flow resistance for VES is believed to be caused by the formation of transient shear induced structures [61]. Surprisingly, for both HPAM and VES *the critical shear rate, after which the flow resistance increases rapidly (around 6 s^{-1} for HPAM and 25 s^{-1} for VES), directly corresponds to the critical Ca number (4×10^{-5} for HPAM and 7×10^{-5} for VES respectively) where the oil saturation decreases rapidly*. At such shear rates the value of the mobility ratio *M* for VES is around unity. For HPAM this critical shear rate corresponds to a De number of around 2. As shown in table 1, the relaxation time of xanthan is an order of magnitude lower than that of HPAM. Thus at similar shear rate the Elasticity number $\left(El = De/\mathrm{Re}\right)$, is much higher for HPAM than for xanthan. As the elasticity number is independent of the flow kinematics and depends only on the fluid rheology and the characteristic size of the porous medium, a higher elasticity number essentially means that stronger elastic effects are expected in HPAM compared to the shear thinning xanthan fluid. Our observation regarding HPAM and xanthan closely correlate with the recent findings of Clarke et al. [18,59] and Howe et al. [19]. We hypothesize that the velocity and pressure fluctuations, and possible presence of transversal flows, at these higher De numbers cause stronger fluctuations in the interface of the larger oil ganglia. This will enable the flow to break up larger oil ganglia into smaller droplets. The instability will moreover facilitate to mobilize the small droplets. The water and pseudoplastic shear thinning xanthan solution do not create such elastic instabilities, even at higher shear rates. This work has added evidence of this elastic micro-sweep mechanism by analyzing the oil ganglia size distributions for the different types of displacement fluids, showing that much larger residual oil droplet sizes remain when using water and xanthan solutions.

4 Conclusion

Summary, hypothesis, new concepts, innovations

It is of primary importance to understand the effect of fluid rheology and fluid solid interaction in multiphase flow through porous media. Water, pseudoplastic shear-thinning xanthan, viscoelastic HPAM, and viscoelastic surfactants are extensively used as displacing fluids in different stages of oil recovery. In this work, we have used a microchannel with a regular arrangement of pillars as a tool to visualize and understand the enhanced oil recovery process. For a similar range of Ca numbers, under our experimental conditions we found that the HPAM solution and viscoelastic surfactants can displace more oil compared to shear thinning xanthan or water. Digging deeper into the enhanced recovery phenomenon, we showed that the typical residual droplet size for HPAM and VES is much smaller, compared to xanthan or water, at higher Ca numbers. Although the mobility ratio of both water and VES is less than 1, VES shows a much larger oil displacement than water. The droplet size distribution analysis provides

a detailed insight into how viscoelastic effects can significantly affect the droplet size distribution compared to xanthan with a similar shear thinning behavior. The critical Ca number beyond which the residual oil saturation decreases rapidly for HPAM and VES corresponds to the critical shear rate where both fluids show an increased viscosity in single phase flow through the same porous medium. This proves that elastic effects, which initiate strong spatial and temporal fluctuations, play a crucial role to break larger ganglia to smaller micro droplets and can mobilize the micro droplets.

Key improvements compared to earlier literature

This micro-sweep mechanism is different from earlier findings in the literature [16]. Wang et al. [62] proposed that a pulling effect mechanism by elastic fluids can be the cause of excess recovery. The excess flow resistance or shear thickening effect for flow of single phase viscoelastic fluids through porous medium is also hypothesized to be a possible mechanism of microscopic displacement by several researchers [45,63]. However no direct correlation have been presented [16]. Very recently Clarke et al [18] proposed that elastic instability can be a possible mechanism for excess recovery for HPAM fluids. In this study we confirm and extend the work of Clarke et al. [18], and for the first time show a quantitative size distribution of residual oil ganglia after sweeping by different displacing fluids. Rodriguez de Castro et al. [46] very recently showed the effect of shear thinning xanthan of different concentrations on residual oil distribution. However, we present a comparative recovery performance of xanthan, HPAM, VES and Newtonian water solution in a similar range of Ca number. Through an analysis of the critical Ca number for desaturation and the residual droplet size distribution, we demonstrate that viscoelastic surfactants can also be used as a potential displacing fluid, along with HPAM, and that the excess recovery is related to elastic effects [39]. In case of oil field applications, the displacement experiments with polymeric fluids are mostly performed in core samples extracted from the field. Such experiments provide a correlation between the applied flow rate and residual oil saturation, but a detailed inspection of the flow structures at the pore level is very difficult [47,64,65]. Our experimental findings and analysis of residual oil droplet size distribution for different non-Newtonian displacing fluids, and its correlation to elastic instability, is extremely important as all the fluids studied in this work are used for enhanced oil recovery and other crucial applications involving multiphase flow through porous media. Knowledge from this study will further enable to synthesize and optimize smart polymeric agents for related applications.

Future work

Our pillared microchannels are hydrophilic in nature. Hydrophilic rock surface may create a thin layer of displacement fluid between the oil and the porous medium surface, which may act as a lubricating layer that can enhance the displacement efficiency. So our results mostly apply to the case of hydrophilic rock formations. Our finding can be useful to optimize parameters in the reservoir simulation software and moreover synthesize better polymers for enhanced oil recovery and other industrial and environmental applications. We have performed our experiments in a 2D model porous medium using a quite diverse, but still specific, set of displacement fluids and concentrations. To obtain a complete understanding we would like to

study a 3D porous medium with a more complex geometric configuration (similar to a representative real rock structure), using a larger set of fluids, and compare with our current observations and numerical simulations in the future.

Acknowledgements

References

[1] F.A.L. Dullien, Porous Media-Fluid Transport and Pore Structure, Academic, New York, 1979.

[2] G. Lake, L.W., Johns, R.T., Rossen, W.R. and Pope, Fundamentals of enhanced oil recovery., Society of Petroleum Engineers, 1986.

[3] H. Khosravian, V. Joekar-niasar, N. Shokri, Transport Phenomena and Fluid Mechanics Effects of Flow History on Oil Entrapment in Porous Media : An Experimental Study, AIChE Journal 61.4 (2015) 1385–1390. doi:10.1002/aic.

[4] B. Zhao, C.W. Macminn, R. Juanes, Wettability control on multiphase flow in patterned microfluidics, Proceedings of the National Academy of Sciences.113.37 (2016). doi:10.1073/pnas.1603387113.

[5] J. Beaumont, H. Bodiguel, A. Colin, Drainage in two-dimensional porous media with polymer solutions, Soft Matter. 9 (2013) 10174. doi:10.1039/c3sm51480c.

[6] G. Lo, Interface scaling in a two-dimensional porous medium under combined viscous , gravity , and capillary effects, Physical Review E. 66 (2002) 1–12. doi:10.1103/PhysRevE.66.051603.

[7] G. Løvoll, Y. Méheust, R. Toussaint, J. Schmittbuhl, K.J. Måløy, Growth activity during fingering in a porous Hele-Shaw cell, Phys. Rev. E 70 (2004) 1–12. doi:10.1103/PhysRevE.70.026301.

[8] M.M. Dias, A.C. Payatakes, Network models for two-phase flow in porous media Part 1. Immiscible microdisplacement of non-wetting fluids, J. Fluid Mech. 164 (1986) 305. doi:10.1017/S0022112086002574.

[9] K. Ma, J. Rivera, G.J. Hirasaki, S.L. Biswal, Wettability control and patterning of PDMS using UV-ozone and water immersion, J. Colloid Interface Sci. 363 (2011) 371–378. doi:10.1016/j.jcis.2011.07.036.

[10] M. Sahimi, Flow phenomena in rocks : from continuum models to fractals , percolation, cellular automata , and simulated annealing, Reviews of modern physics 65 (1993) 1393.

[11]   R. Lenormand, E.Touboul, and C. Zarcone. Numerical models and experiments on immiscible displacements in porous media. Journal of fluid mechanics, 189 (1988) 165-18

[12]   A. Afsharpoor, M.T. Balhoff, Static and Dynamic CFD Modeling of Viscoelastic Polymer: Trapped Oil Displacement and Deformation at the Pore-Level, SPE Annu. Tech. Conf. Exhib. (2013) 166114. doi:10.2118/166114-MS.

[13]   M. Hashemi, M. Sahimi, Dynamics of Two-Phase Flow in Porous Media : Simultaneous Invasion of Two Fluids. AIChE journal 45 (1999) 1365–1382.

[14]   J. Heemskerk, R. Janssen-van Rosmalen, R.J. Holtslag, D. Teeuw, Quantification of Viscoeleastic Effects of Polyacrylamide Solutions, SPE/DOE Fourth Symp. Enhanc. Oil Recover. (1984) 1–8. doi:10.2118/12652-MS.

[15]   A. Rodríguez de Castro, N. Shokri, N. Karadimitriou, M. Oostrom, & V . Joekar-Niasar. Experimental study on nonmonotonicity of Capillary Desaturation Curves in a 2-D pore network. Water Resources Research, 51 (2015) 8517-8528.

[16]   D. Rodrigue, B.W.L. Romero-zero, Oil displacement mechanisms of viscoelastic polymers in enhanced oil recovery (EOR): a review, Journal of Petroleum Exploration and Production Technology. 4 (2014) 113–121. doi:10.1007/s13202-013-0087-5.

[17]   L.Guan, Y.Du, Field-scale polymer flooding: lessons learnt and experiences gained during past 40 years, SPE Int. Pet. Conf. Mex. Soc. Pet. Eng. (2004).

[18]   A. Clarke, A.M. Howe, J. Mitchell, J. Staniland, L. Hawkes, K. Leeper, Mechanism of anomalously increased oil displacement with aqueous viscoelastic polymer solutions., Soft Matter. 11 (2015) 3536–41. doi:10.1039/c5sm00064e.

[19]   A.M. Howe, A. Clarke, D. Giernalczyk, Flow of concentrated viscoelastic polymer solutions in porous media: effect of M W and concentration on elastic turbulence onset in various geometries, Soft Matter. 11 (2015) 6419–6431. doi:10.1039/C5SM01042J.

[20]   J. Mitchell, K. Lyons, A.M. Howe, A. Clarke, Viscoelastic polymer flows and elastic turbulence in three-dimensional porous structures, | Soft Matter Soft Matter. 12 (2016) 460–468. doi:10.1039/c5sm01749a.

[21]   M. Lotfollahi, H. Koh, Z. Li, M. Delshad, G.A. Pope, Mechanistic Simulation of Residual Oil Saturation in Viscoelastic Polymer Floods, SPE EOR Conf. Oil Gas West Asia, Muscat, Oman. (2016). doi:10.2118/179844-MS.

[22]   P. Qi, D.H. Ehrenfried, H. Koh, M.T. Balhoff, Reduction of Residual Oil Saturation in Sandstone Cores using Viscoelastic Polymers, SPE Improv. Oil Recover. Conf. Held Tulsa, Oklahoma,USA. (2016) 1–16. doi:SPE-179689-MS.

[23]   S.S. Datta, T.S. Ramakrishnan, D.A. Weitz, Mobilization of a trapped non-wetting fluid from a three-dimensional porous medium, Phys. Fluids. 26 (2014) 022002. doi:10.1063/1.4866641.

[24]   A. Groisman, V. Steinberg, Elastic turbulence in a polymer solution flow, Nature. 405 (2000) 53–55. doi:10.1038/35011019.

[25]   S. De, J.A.M. Kuipers, E.A.J.F. Peters, J.T. Padding, Viscoelastic flow simulations in

model porous media, Phys. Rev. Fluids. 2 (2017) 53303. doi:10.1103/PhysRevFluids.2.053303.

[26] E.S. Shaqfeh, Fully Elastic Instabilities in Viscometric Flows, Annu. Rev. Fluid Mech. 28 (1996) 129–185. doi:10.1146/annurev.fluid.28.1.129.

[27] R.J. Poole, M.A. Alves, P.J. Oliveira, Purely elastic flow asymmetries, Phys. Rev. Lett. 99 (2007) 1–4. doi:10.1103/PhysRevLett.99.164503.

[28] J. Zilz, R.J. Poole, M.A. Alves, D. Bartolo, B. Levache, A. Lindner, Geometric scaling of a purely elastic flow instability in serpentine channels, J. Fluid Mech. 712 (2012) 203–218. doi:10.1017/jfm.2012.411.

[29] P. Pakdel, G.H. McKinley, Cavity flows of elastic liquids: Purely elastic instabilities, Phys. Fluids. 10 (1998) 1058–1070. doi:10.1063/1.869631.

[30] L. Pan, A. Morozov, C. Wagner, P.E. Arratia, Nonlinear elastic instability in channel flows at low reynolds numbers, Phys. Rev. Lett. 110 (2013) 1–5. doi:10.1103/PhysRevLett.110.174502.

[31] P. Pakdel, G. McKinley, Elastic Instability and Curved Streamlines, Phys. Rev. Lett. 77 (1996) 2459–2462. doi:10.1103/PhysRevLett.77.2459.

[32] S. De, J. van der Schaaf, N. G. Deen, J. A. M. Kuipers, E. A. J. F. Peters and J.T. Padding, Elastic Instabilities in Flows through Pillared Micro channels, arXiv Prepr. arXiv. 1607.03672 (2016), submitted to Physics of Fluids (2017).

[33] Y. Zhao, A.Q. Shen, S.J. Haward, Flow of wormlike micellar solutions around confined microfluidic cylinders, Soft Matter. 12 (2016) 8666–8681. doi:10.1039/C6SM01597B.

[34] J.J. Cardiel, A.C. Dohnalkova, N. Dubash, Y. Zhao, P. Cheung, A.Q. Shen, Microstructure and rheology of a flow-induced structured phase in wormlike micellar solutions., Proc. Natl. Acad. Sci. U. S. A. 110 (2013) E1653-60. doi:10.1073/pnas.1215353110.

[35] Y. Zhao, P. Cheung, A.Q. Shen, Microfluidic flows of wormlike micellar solutions, Advances in colloid and interface science. 211 (2014) 34–46. doi:10.1016/j.cis.2014.05.005.

[36] M.R. Rojas, A.J. Müller, A.E. Sáez, Shear rheology and porous media flow of wormlike micelle solutions formed by mixtures of surfactants of opposite charge, J. Colloid Interface Sci. 326 (2008) 221–226. doi:10.1016/j.jcis.2008.07.022.

[37] S.J. Haward, T.J. Ober, M.S.N. Oliveira, M. a. Alves, G.H. McKinley, Extensional rheology and elastic instabilities of a wormlike micellar solution in a microfluidic cross-slot device, Soft Matter. 8 (2012) 536–555. doi:10.1039/c1sm06494k.

[38] S.J. Haward, F.J. Galindo-rosales, P. Ballesta, M.A. Alves, microchannels Spatiotemporal flow instabilities of wormlike micellar solutions in rectangular microchannels, Applied Physics Letters. 124101 (2014). doi:10.1063/1.4869476.

[39] S. De, M. Golombok, S.P. Koesen, R.V. Maitri, J.T. Padding, J.F.M. van Santvoort, Flow of viscoelastic surfactants through porous media, accepted in AIChE J. (2017).

10.1002/aic.15960.

[40] S. De, S. Das, J.A.M. Kuipers, E.A.J.F. Peters, J.T. Padding, A coupled finite volume immersed boundary method for simulating 3D viscoelastic flows in complex geometries, J. Nonnewton. Fluid Mech. 232 (2016) 67–76. doi:10.1016/j.jnnfm.2016.04.002.

[41] A.W. Liu, D.E. Bornside, R.C. Armstrong, R.A. Brown, Viscoelastic flow of polymer solutions around a periodic, linear array of cylinders: comparisons of predictions for microstructure and flow fields, J. Nonnewton. Fluid Mech. 77 (1998) 153–190. doi:10.1016/S0377-0257(97)00067-0.

[42] B. Khomami, L.D. Moreno, Stability of viscoelastic flow around periodic arrays of cylinders, Rheol. Acta. 36 (1997) 367–383. doi:10.1007/BF00396324.

[43] S. De, J.A.M. Kuipers, E.A.J.F. Peters, J.T.Padding, Viscoelastic flow simulations in random porous media, J. Nonnewton. Fluid Mech. 248 (2017) 50-61.

[44] J. Avendano, N. Pannacci, B. Herzhaft, P. Gateau, P. Coussot, Journal of Colloid and Interface Science Enhanced displacement of a liquid pushed by a viscoelastic fluid, J. Colloid Interface Sci. 410 (2013) 172–180. doi:10.1016/j.jcis.2013.08.014.

[45] M.A. Nilsson, R. Kulkarni, L. Gerberich, R. Hammond, R. Singh, E. Baumhoff, J.P. Rothstein, Effect of fluid rheology on enhanced oil recovery in a microfluidic sandstone device, J. Nonnewton. Fluid Mech. 202 (2013) 112–119. doi:10.1016/j.jnnfm.2013.09.011.

[46] A. Rodríguez, D. Castro, M. Oostrom, N. Shokri, Journal of Colloid and Interface Science Effects of shear-thinning fluids on residual oil formation in microfluidic pore networks, 472 (2016) 34–43. doi:10.1016/j.jcis.2016.03.027.

[47] Victor Lifton, 2016 Microfluidics an enabling screening technology for enhanced oil recovery (EOR), Lab on a Chip. 16 (2016) 1–43. doi:10.1039/C6LC00318D

[48] H. Emami, M. Riyaz, Study of Microscopic and Macroscopic Displacement Behaviors of Polymer Solution in Water-Wet and Oil-Wet Media, Transport in porous media. 89 (2011) 97–120. doi:10.1007/s11242-011-9754-5.

[49] K. Ma, R. Liontas, C.A. Conn, G.J. Hirasaki, S.L. Biswal, Visualization of improved sweep with foam in heterogeneous porous media using microfluidics, Soft Matter. 8 (2012) 10669–10675. doi:10.1039/c2sm25833a.

[50] S.R.A. De Loos, J. Van Der Schaaf, R.M. Tiggelaar, T.A. Nijhuis, M.H.J.M. De Croon, J.C. Schouten, Gas-liquid dynamics at low Reynolds numbers in pillared rectangular micro channels, Microfluid. Nanofluidics. 9 (2010) 131–144. doi:10.1007/s10404-009-0525-3.

[51] A. Palaniraj, V. Jayaraman, Production, recovery and applications of xanthan gum by Xanthomonas campestris, J. Food Eng. 106 (2011) 1–12. doi:10.1016/j.jfoodeng.2011.03.035.

[52] L. Zhong, M. Oostrom, M.J. Truex, V.R. Vermeul, J.E. Szecsody, Rheological behavior of xanthan gum solution related to shear thinning fluid delivery for subsurface

remediation, J. Hazard. Mater. 244–245 (2013) 160–170. doi:10.1016/j.jhazmat.2012.11.028.

[53] R.B. Bird, R.C. Armstrong, O. Hassager, Dynamics of polymeric liquids. Vol. 1, 2nd Ed. : Fluid mechanics, 1987.

[54] S.V.G. Menon, P.S. Goyal, B.A. Dasannacharya, S.K. Paranjpe, R. V. Mehta, R. V. Upadhyay, When does a living polymer live? - Case of CTAB/NaSal, Phys. B Phys. Condens. Matter. 213–214 (1995) 604–606. doi:10.1016/0921-4526(95)00225-X.

[55] G.R. Moss, J.P. Rothstein, Flow of wormlike micelle solutions past a confined circular cylinder, J. Nonnewton. Fluid Mech. 165 (2010) 1505–1515. doi:10.1016/j.jnnfm.2010.07.014.

[56] J.P. Rothstein, Strong Flows of Viscoelastic Wormlike Micelle Solutions, Rheol. Rev. 2008 (2008) 1–46..

[57] P.C. Sousa, F.T. Pinho, M.S.N. Oliveira, M.A. Alves, Efficient microfluidic rectifiers for viscoelastic fluid flow, J. Nonnewton. Fluid Mech. 165 (2010) 652–671. doi:10.1016/j.jnnfm.2010.03.005.

[58] G.E. Meyer, J.C. Neto, Verification of color vegetation indices for automated crop imaging applications, Comput. Electron. Agric. 63 (2008) 282–293. doi:10.1016/j.compag.2008.03.009.

[59] A. Clarke, A.M. Howe, J. Mitchell, J. Staniland, L.A. Hawkes, How Viscoelastic-Polymer Flooding Enhances Displacement Efficiency, SPE J. 21 (2016) 0675–0687. doi:10.2118/174654-PA.

[60] D. Kawale, E. Marques, P.L.J. Zitha, M.T. Kreutzer, W.R. Rossen, P.E. Boukany, Elastic instabilities during the flow of hydrolyzed polyacrylamide solution in porous media: effect of pore-shape and salt, Soft Matter. 24 (2017) 765-775. doi:10.1039/C6SM02199A.

[61] Y. Zhao, A.Q. Shen, S.J. Haward, Flow of wormlike micellar solutions around confined microfluidic cylinders, Soft Matter. 12 (2016) 8666–8681. doi:10.1039/C6SM01597B.

[62] H. Wang, D., Wang, G., Wu, W., Xia, H., & Yin, The Influence of Viscoelasticity on Displacement Efficiency-From Micro to Macro Scale., SPE Annu. Tech. Conf. Exhib. Soc. Pet. Eng. (2007).

[63] W.M. Jones, Polymer additives in reservoir flooding for oil recovery: shear thinning or shear thickening?, J. Phys. D. Appl. Phys. 13 (1980) 87–88. doi:10.1088/0022-3727/13/5/004.

[64] R.P. Chhabra, J. Comiti, I. Machao, Flow of non-Newtonian fluids in fixed and fluidised beds, Chem. Eng. Sci. 56 (2001) 1–27. doi:10.1016/S0009-2509(00)00207-4.

[65] T.S. Urbissinova, J.J. Trivedi, E. Kuru, Effect of elasticity during viscoelastic polymer flooding: A possible mechanism of increasing the sweep efficiency, J. Can. Pet. Technol. 49 (2010) 49–56. doi:10.2118/133471-PA.

List of Figure captions:

Figure 1. Geometry of the pillared microchannel: (a) channel geometry with dots showing the pillar locations. Flow is from left to right (x-direction). Planar walls are present at both sides in the width (y) and height (z) direction; (b) arrangement of pillars, indicating the distances between pillars X_p and Y_p; (c) SEM image of a typical pillared channel (arrangement and structure of a typical pillar is shown)

Figure 2. Steady shear viscosity vs. shear rate for the xanthan solution, fitted with the CY model

Figure 3. Steady shear viscosity vs. shear rate for the HPAM solution, fitted with the CY model

Figure 4. Steady shear viscosity vs. shear rate for the VES solution

Figure 5. Percentage remaining oil saturation as a function of capillary number for different displacing fluids. Error bars show the variability between 3 experiments.

Figure 6. Snapshots of residual oil microstructures in steady state after displacement by (a) water, (b) xanthan, (c) HPAM, and (d) VES. The subfigures (1, 2 and 3) correspond to increasing Ca numbers.

Figure 7. Steady state residual oil size distribution after displacement by (a) water, (b) xanthan, (c) HPAM, and (d) VES. Different colors correspond to difference Ca numbers.

Figure 8. Apparent viscosity from single phase flow through the pillared microchannel (red circles) and from the shear rheometer (black circles) as a function of (apparent) shear rate for different displacing fluids: (a) xanthan, (b) HPAM, (c) VES.

List of Tables:

Table 1. Rheological parameters from Carreau – Yasuda model

Fluids	λ (s)	n	a	η_0 (Pa.s)	η_∞ (Pa.s)
Xanthan	5.0×10^{-2} $\pm 1.0\times10^{-3}$	2.5×10^{-1} $\pm 5.0\times10^{-3}$	6.2×10^{-1} $\pm 4.0\times10^{-3}$	4.9×10^{-2} $\pm 2.0\times10^{-4}$	1.0×10^{-3}
HPAM 3630	3.0×10^{-1} $\pm 2\times10^{-2}$	5.8×10^{-1} $\pm 1\times10^{-2}$	1.07 $\pm 7\times10^{-2}$	5.0×10^{-2} $\pm 4.0\times10^{-4}$	1.0×10^{-3}